Current Applied Physics 16 (2016) 914–921

Contents lists available at ScienceDirect

Current Applied Physics

journal homepage: www.elsevier.com/locate/cap

Synthesis of hierarchical CuO nanostructures: Biocompatible antibacterial agents for Gram-positive and Gram-negative bacteria

S. Sonia [a, b], R. Jayasudha [c], Naidu Dhanpal Jayram [a, d], P. Suresh Kumar [e], D. Mangalaraj [a, *], S.R. Prabagaran [c]

[a] Department of Nanoscience and Technology, Bharathiar University, Coimbatore, 641 046, India
[b] Department of Physics, Holy Cross College (Autonomous), Nagercoil, 6410046, India
[c] Department of Biotechnology, Bharathiar University, Coimbatore, 641046, India
[d] Department of Science and Humanities, Kalaignar Karunanidhi Institute of Technology, Kannampalayam, Coimbatore, Tamil Nadu, 641402, India
[e] Environmental and Water Technology, Center of Innovation, Ngee Ann Polytechnic, Singapore, 599489, Singapore

ARTICLE INFO

Article history:
Received 23 January 2016
Received in revised form
1 May 2016
Accepted 10 May 2016
Available online 11 May 2016

Keywords:
CuO nanostructures
High surface area
Antibacterial activity
Human pathogens

ABSTRACT

Hierarchical cupric oxide (CuO) nanostructures (such as nanoflowers, nanorods, nanoleaves and nanoflakes) were synthesized by low temperature sonochemical method and studied its biocompatible and antibacterial functionality. The antibacterial activity of CuO nanostructures in three different concentrations (12.5 μg/ml, 25 μg/ml and 50 μg/ml) have been studied through agar diffusion method against four pathogenic bacteria viz., *Staphylococcus aureus*, *Streptococcus pneumoniae*, *Salmonella typhimurium*, and *Serratia marcescens*. Nanoflowers exhibited more antibacterial activity than nanorods, nanoleaves and nanoflakes, which may be of high specific surface area of nanoflowers (58.63 m^2/g). The minimum inhibitory concentration (MIC) for all the compounds is 12.5 μg/ml and showed the maximum zone of inhibition (43 ± 0.5 mm) at 50 μg/ml concentration. Hence our study strongly proved that the synthesized CuO nanostructures can act as excellent antibacterial agents towards human pathogens.

1. Introduction

Metal oxide nanostructures have stimulated great interest in the field of environmental remediation due to their salient features such as abundance, high stability, and tunable optical and structural properties. The current interest of miniaturization is to develop a protocol for controlled growth of metal oxide nanostructures with desired size and shape for exploring novel applications. Antibacterial activity is one important area, which influences the environmental remediation in various aspects. Antimicrobial agents are of high relevance in numerous commercial applications such as in food industries, textiles and medical products [1]. However random use of antibiotics has triggered the bacterial resistance against many antimicrobial drugs, which necessitates the greater need for newer antimicrobial agents to which bacteria would not develop resistance. The antibacterial activity has been observed to vary-with respect to surface area of the material, therefore the inorganic nanomaterials with different morphologies (different surface area) can be used in broad range of reactions. CuO has good antibacterial activity, which is classified in a group of inorganic antimicrobial agents [2], they are safer and extremely stable compared to organic microbial agents. Surface area, surface defects and Reactive Oxygen Species (ROS) produced from the material play an important role in the antibacterial activity of semiconductors. The synthesis of CuO antibacterial agents with large surface area would be of great significance to meet out our challenges.

Copper Oxide is one of the important materials among the most widely applied antimicrobial agents such as silver, zinc oxide, and titanium dioxide etc. Although copper oxide displays antibacterial activity towards microorganisms, it showed insignificant lethal activity against bacterial eradication [3–6]. In addition, previous studies failed to determine the mechanism behind antimicrobial action of CuO nanoparticles (CuO NPs). Similarly, biocompatibility of antimicrobial agents has not been studied; it is one of the key challenges toward assessment of their environmental impact. But our study reports the biocompatibility, and shape dependent antibacterial action of nanostructured CuO, and their mechanistic

* Corresponding author.
E-mail addresses: sureshinphy@yahoo.com (P.S. Kumar), dmraj800@yahoo.com (D. Mangalaraj).

http://dx.doi.org/10.1016/j.cap.2016.05.006
1567-1739/

action towards pathogenic bacterial strains. It is observed that, the surface property is highly dependent on the shape of the nanostructures. CuO NPs also have an adverse effect on bacteria, Cu^{2+} dissolving from CuO NPs induce toxic effects by triggering ROS production and DNA damage in bacteria [7]. It has been realized that CuO could serve as an inexpensive and effective antimicrobial agent owing to its ionization property. Cost-wise, it is cheaper than silver, and relatively stable in terms of both chemical and physical properties. The present work was intended to synthesis effective CuO nanostructure using simple and facile chemical routes and study the antibacterial activity towards both Gram positive and Gram negative strains (such as, *Staphylococcus aureus*, *Streptococcus pneumoniae*, *Salmonella typhimurium* and *Serratia marcescens*).

2. Experimental

2.1. Materials

Copper acetate ($Cu(CH_3COO)_2 \cdot 2H_2O$), sodium hydroxide (NaOH), tri-sodium citrate ($Na_3C_6H_5O_7$), ammonia (NH_3), citric acid ($C_6H_8O_7$), and ethylene glycol ($C_2H_6O_2$) were procured from Himedia at analytical grade, and used for synthesis of the CuO nanostructures without any further purification.

2.2. Synthesis of copper oxide (CuO) nanostructures

CuO nanorods and nanoleaves were prepared through chemical route as reported in our previous work [8,9]. In a typical synthesis of nanoflowers, Cu^{2+} precursor Cu $(CH_3COO)_2$. $2H_2O$ (0.1 M) was dissolved in distilled water and 3 ml of NH_3 was added drop wise under magnetic stirring. After homogeneous mixing, 3 g of citric acid was introduced in the reaction mixture. Then, the solution was heated in a Teflon case at 160 °C for 12 h and cooled to room temperature naturally. The obtained black color precipitate was collected, and washed with water and ethanol for several times and then dried at 80 °C for 6 h. In the case of nanoflakes, 0.2 M of copper acetate and 0.5 M of NaOH solutions were prepared in distilled water. Subsequently, NaOH solution was slowly added to the copper acetate solution under stirring to obtain homogeneous solution. Then, 1 g of citric acid and two different volumes (10 and 20 ml) of ethylene glycol were added drop wise in the above solution and the resultant solution was loaded into a 75 ml Teflon – lined autoclave. Finally, the autoclave was sealed and maintained at 160 °C for 12 h. It was then allowed to cool down to room temperature naturally. The precipitate was filtered, and then washed with distilled water to remove soluble acetate and with ethanol to reduce agglomeration and dried at 80 °C for 6 h.

2.3. Antibacterial activity test

In the present study, the agar well diffusion method has been applied to evaluate the antibacterial activity, which is one of the non automated in-vitro bacterial susceptibility tests. This method produces zone of clearance in mm due to the growth inhibition activity of antimicrobial agents. Luria Bertani (LB) agar with 1 g of Peptone, 0.5 g of Yeast extract, 1 g of Sodium chloride (NaCl), 2 g of Agar, and 100 ml of Distilled water was prepared and then sterilized in an autoclave at 15 lbs pressure and 121 °C for 15 min. Subsequently, the sterilized medium (50 ml) was poured into sterile petri dishes (26 mm) under aseptic condition. Bacterial inoculum of *Staphylococcus aureus* (ATCC 25923), *Streptococcus Pneumoniae* (ATCC 49619), *Salmonella typhimurium* (Clinical isolate), and *Serratia marcescens* (NRRL 2544) was prepared by inoculating loopful of the respective bacteria in 5 ml of Luria Bertani broth and incubated at 37 °C till the turbidity matched with 0.5 Mac-Farland standard. The prepared LB agar plates were inoculated with the above test organisms by spreading the bacterial inoculum on the surface of the medium. Then wells (8 mm in diameter) were punched in the agar and the prepared nano-materials at different concentrations (12.5 μg/ml, 25 μg/ml and 50 μg/ml) were added into the well. After the incubation period (18–24 h), the zone of inhibition for each compounds was measured in mm.

2.4. Hemolytic assay

Freshly collected blood (4 ml) was subjected to density gradient centrifugation using phosphate buffer solution. The red blood corpuscles (RBCs) were carefully collected and washed 4 times using phosphate buffer saline (PBS) at 3000 rpm for 15 min. The washed RBC was diluted with 40 ml PBS. 0.2 ml of diluted RBC was added with the nanoparticle suspension in PBS and centrifuged at 10,000 rpm for 15 min and the supernatant (1 ml) was collected. The absorbance of hemoglobin was measured. Here, RBC diluted with water was used as a positive control and RBC diluted with PBS was used as a negative control.

$$\text{Hemolysis (\%)} = (A_{\text{sample}} - A_{-\text{ve control}})/(A_{+\text{ve control}} - A_{-\text{ve control}}) \times 100$$

2.5. Characterization techniques

A PAN analytical (X-Pert-Pro) X-ray diffractometer using Cu $K\alpha_1$ radiation (λ = 1.5406 Å) was employed to characterize the crystallographic properties of the CuO nanostructures. FT-IR analysis was performed by Bruker Tensor 27, Fourier Transforms Infrared Spectroscope. The surface morphologies were characterized by a FEI Quanta – 250 Field Emission Scanning Electron Microscopy (FESEM). Particle size distribution (PSD) was assessed in a Zeta Sizer Nano (Malvern Instruments, West borough, MA). This instrument measures Dynamic light scattering process (DLS) (173°) of nanoparticles in the range of 100–6000 nm by backscattering. The same instrument was used to measure the zeta potential of nanoparticles suspensions. Nitrogen adsorption-desorption isotherms of the present study were obtained using Autosorb –1 (Quantachrome instrument).

3. Results and discussion

3.1. Structural analysis

The powder XRD pattern of the different morphologies of CuO is shown in Fig. 1a. All the diffraction peaks are well matching with the standard JCPDS (05–0661) data and their lattice constants are calculated as, a = 4.68 Å, b = 3.42 Å and c = 5.13 Å. The major peaks located at 2θ = 35.43° and 38.49° are indexed as (002) and (111) planes respectively and which confirmes the monoclinic structure of the CuO (Fig. 1a). The average grain size of the copper oxide nanostructures is calculated by Scherrer formula [10]. The average grain size was found to be 50, 35, 17 and 49 nm for nanoflowers, nanorods, nanoleaves and nanoflakes respectively. The sharp and narrow diffraction peaks of nanoflowers indicate that the nanoflowers have high crystalline nature. No characteristic peaks from the intermediates such as $Cu(OH)_2$ was detected in the XRD pattern. The composition and quality of the copper oxide nanostructures such as nanoflowers, nanorods, nanoleaves and nanoflakes were further analyzed by Fourier Transform Infrared spectroscopy (FTIR), in the range of 400–4000 cm^{-1} (Fig. 1b). The absorption bands due to the Cu-O bond in CuO are observed at 430, 507, and 606 cm^{-1}

[11]. Weak and broad absorption bands at 1637 and 3432 cm^{-1} have been observed due to the existence of water molecules and absorption at 1354 cm^{-1} is due to C-H stretching. The XRD pattern and FTIR spectra confirmed that the synthesized nanostructures are CuO.

3.2. Microstructural analysis

Detailed information about the size and typical morphologies of the synthesized CuO products was obtained by FESEM. Fig. 2(a and b) displays the FESEM images of the CuO nanorods grown at 2.0 M NaOH, with an average diameter of 250 nm and the length of 2 μm. Concentration of NaOH and the consequent sonochemical irradiation of the reaction mixture play an important role in the morphology of nanorods. In this process, the complex ion in the reaction mixture is converted to $Cu(OH)_2$ which then decomposes to form CuO nanorods [12]. Fig. 2(c and d) shows low and high magnification images of CuO nanoleaves obtained through hydrothermal process with 0.1 M concentration of citrate. CuO nanoleaves were formed with a width of 50–100 nm and the length of 250–300 nm Fig. 2(e and f) shows the formation of CuO nanoflowers of 500 nm average size, interestingly, each flower was formed from numerous rods that are fused together. Nanoflakes-like morphology was formed with high transparency in the presence of ethylene glycol (Fig. 2(g and h)). While all these structures were synthesized at the same reaction temperature and time, the additives in the reaction mixture were different. It is important to mention that the structures were well reproducible when the growth parameters were kept unchanged. From Fig. 3, the particle size distribution of different CuO nanostructures has been obtained. The average particle size of the nanoflowers is found to be 436 nm, whereas those of nanoleaves, nanorods and nanoflakes were found to be 240, 332 and 420 nm respectively and which were consistent with FESEM analysis.

3.3. Zeta potential analysis

The stability of nanomaterials in dispersion state is one of the major factors for the biomedical applications of nanoparticles [13]. Hence, we measured the zeta potential of CuO nanostructures in an aqueous dispersion, which is a stability determining parameter for aqueous nanosuspension. For a physically stable nano-suspension, a zeta potential of ± 30 mV is required. The surface charge of different morphologies of CuO is shown in Fig. 3(a–c), where high zeta potential values indicate the good dispersion stability of nanorods, nanoleaves and nanoflowers in water, while the low zeta potential value (−16.8 mV) of nanoflakes indicates the instability. Also, the samples were not precipitated for 3 months, which indicates the stability of prepared CuO nanoparticles for a reasonable period of time. This illustrates that the CuO nanostructures can be used as antibacterial agents as well as in biomedical applications.

The surface area plays a major role in the applications of the nanostructures. The pore size distribution was calculated by Barret-Joyner- Halenda (BJH) method utilizing adsorption or desorption process (Fig. 4). The BJH method revealed that the pore sizes of the CuO nanostructures were approximately between 2 and 50 nm. These CuO nanostructures contain micropores, which provide more efficient path for the reactant molecules to shift toward the surface's active sites [14]. Therefore the nanostructured CuO antibacterial agents can offer a favorable environment for the diffusion of reactive oxygen species. The BET (Brauner Emmet Teller) surface areas of various morphologies of CuO are 58.63, 52.020, 48.370 and 26.704 $m^2\ g^{-1}$ for the nanoflowers, nanorods, nanoleaves and nanoflakes respectively. The adsorption isotherm was found to be of type II, with a hysteresis that is typical for microporous materials. The isotherms for all the nanostructured CuO were of a similar nature. It is expected that the high adsorption property and high surface area of CuO nanostructures may provide more adsorption sites and offer more antibacterial activity.

4. Antibacterial activity of CuO nanostructures

Several significant human pathogens were chosen as experimental microorganisms for the antibacterial activity studies of prepared CuO nanostructures. The antibacterial activity of the CuO nanostructures against such bacterial strains namely, *Staphylococcus aureus*, *Streptococcus pneumoniae*, *Salmonella typhimurium* and *Serratia marcescens* were presented in Fig. 5 and the zone of inhibition diameter is shown in Table 1. The obtained results revealed that all other synthesized nanostructures exhibited antibacterial activity with MIC values ranging from 12.5 μg/ml excepting the nanorods, which showed the antibacterial activity

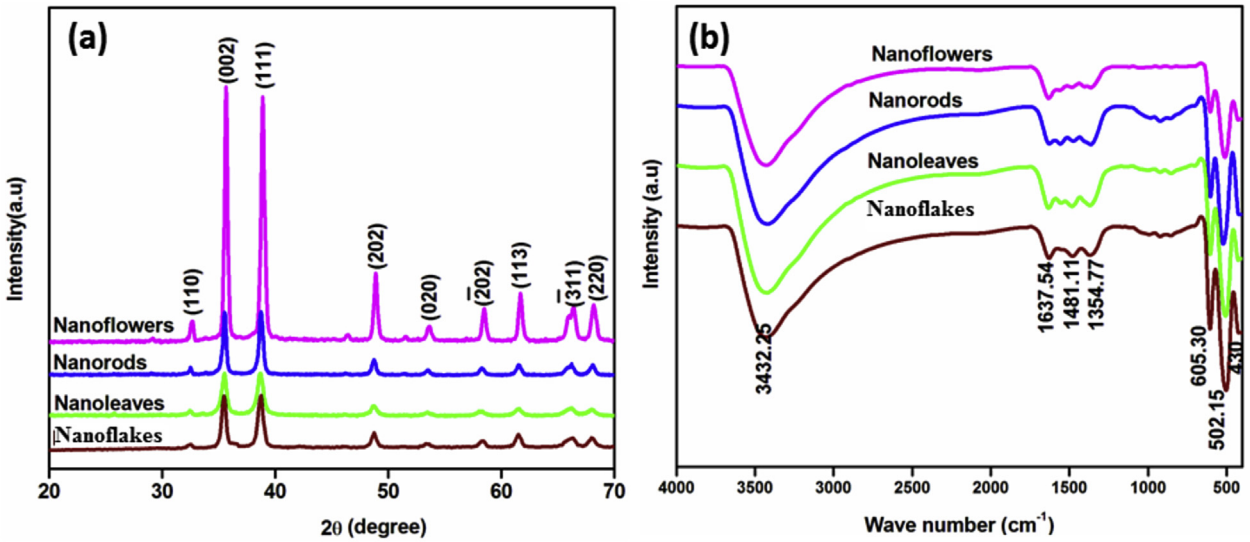

Fig. 1. (a) XRD and (b) FTIR spectra of different CuO nanostructures synthesized via low temperature solution route.

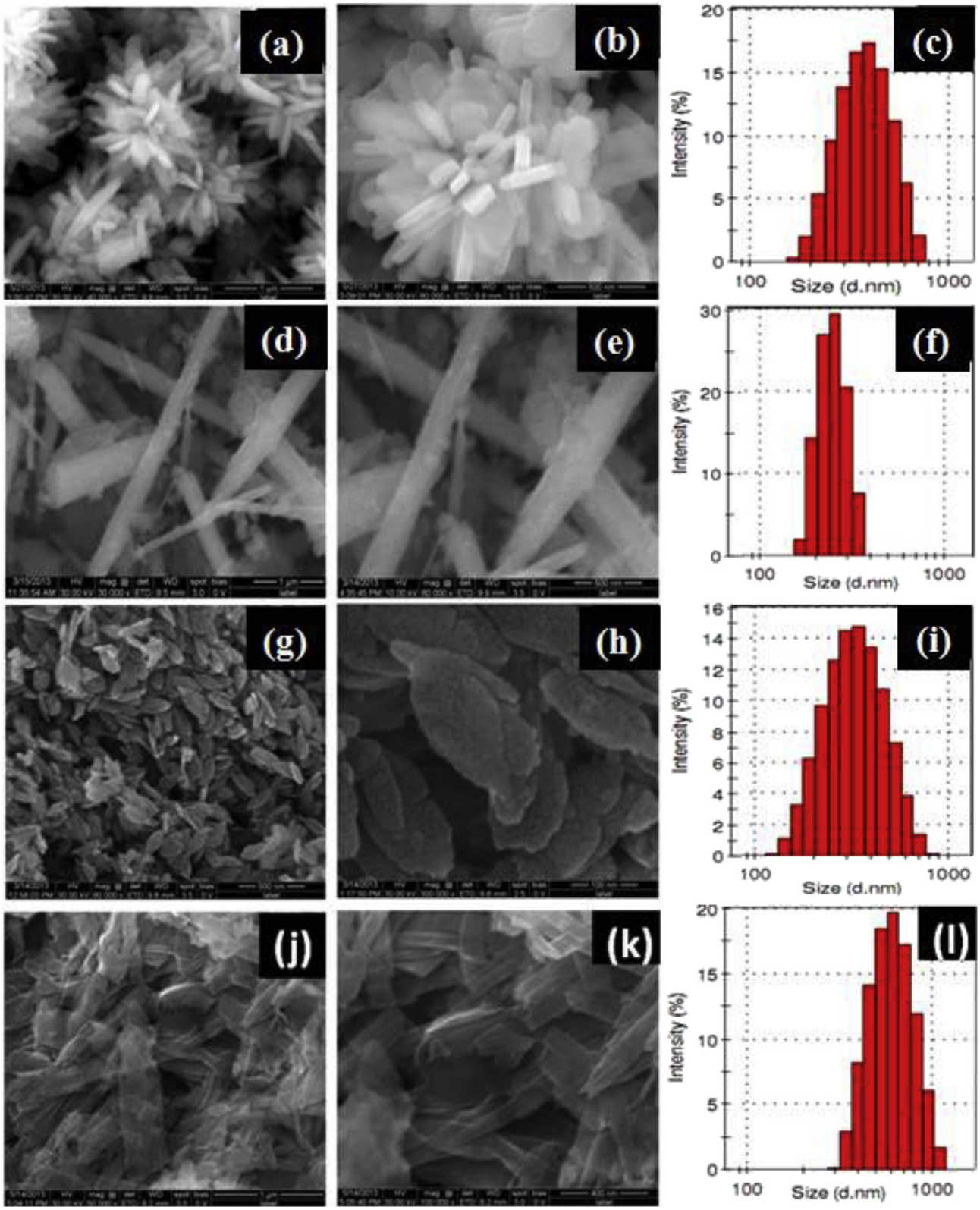

Fig. 2. Low and high magnified FESEM images of different CuO nanostructures (a–b) Nanoflowers (d–e) Nanorods (g–h) Nanoleaves (j–k) Nanoflakes and corresponding (c,f,i,l) Particle Size distribution of CuO nanostructures.

with an MIC value of 25 μg/ml. All the samples showed effective bacterial retardant behavior in the concentration of 50 μg/ml. This indicates that the morphology or the dimensionality of the nanomaterials can immensely affect the antibacterial activity [15]. It is seen that the growth of Gram negative bacterial strains, *Salmonella typhimurium* and *Serratia marcescens* was more effectively

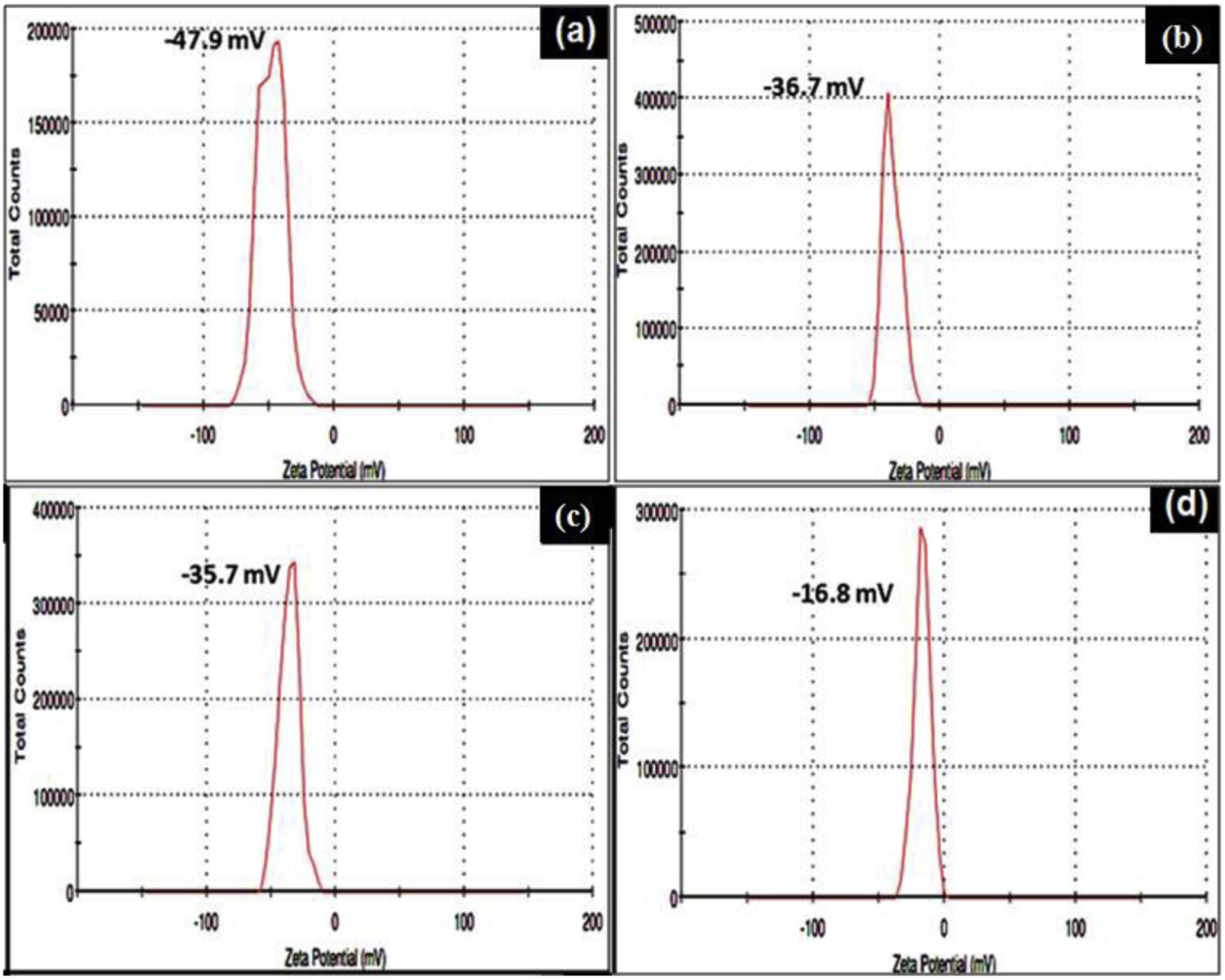

Fig. 3. Zeta potential of different CuO nanostructures (a) Nanoflowers (b) Nanorods (c) Nanoleaves (d) Nanoflakes.

affected by CuO nanostructures than that of the Gram positive strains *Staphylococcus aureus* and *Streptococus pneumoniae* at 50 μg/ml. The difference in activity against these two types of bacteria could be attributed to the structural and compositional differences of the cell membrane [16]. Gram-positive bacteria have thicker peptidoglycan cell membranes compared to the Gram-negative bacteria and it is harder for CuO to penetrate, resulting a low antibacterial response [17]. The antibacterial effect of CuO nanoparticles is due to the generation of reactive oxygen species, which cause bacterial cell damage.

4.1. Antibacterial effect mechanism and biocompatibility study

Generally, toxicity of nanomaterial towards micro-organisms is arises due to the physical disruption and oxidative stress. Previous studies reported that the production of increased levels of reactive oxygen species (ROS) [18,19] and deposition of nanoparticles on the surface of bacteria or accumulation of nanoparticles in the cytoplasm or in the periplasmic region could cause the disorganization of membrane [20]. Since, the ROS, such as hydrogen peroxide (H_2O_2), superoxide anion (O_2^-), hydroxyl radicals (OH_3), and organic hydro peroxides (OHPs) released from nanostructures penetrate into bacteria, they damage cellular constituents such as DNA, lipids, peptidoglycan, and proteins, and destruct cells [21]. However, investigating the nano-biointerface is important to understand the mechanism of bacterial annihilation. Therefore, in the present study, we observed the morphology of bacterial strains before and after exposure to nanostructures with field emission scanning electron microscope (Fig. 6). The killing effect of CuO nanostructures is mainly due to the ROS generation and the release of ionic species.

The cell morphology of bacterial strains before and after exposure to nanostructures (Fig. 6) clearly revealed the interaction of CuO nanostructures and bacterial surface, which caused the disruption of outer membrane and eventually leads to cell death. The close interaction between nanostructures and bacteria imposes a chain reaction starting with the damage and disruption of bacterial membrane (Fig. 6(e–h)). Also we deduce that the high oxidizing power of CuO [22] may produce more number of ROS and lead to lethal activity towards bacterial strains. Additionally, CuO nanostructures has stronger adsorption properties (Fig. 4), resulting in the bacterial cells being adsorbed on to the CuO surface, which increases the contact between bacterium and nanostructures. In this study, nanoflowers showed more antibacterial activity (at 50 μg/ml concentration) than other nanostructures which may be due to the high surface area (58.63 m^2/g). Hence, the different antibacterial activities of the CuO nanostructures are related to their ability to generate such radicals, which is dependent on the surface area and crystal edges exposed. The biocompatibility of CuO nanostructures (50 μg/ml) was analyzed using hemolysis

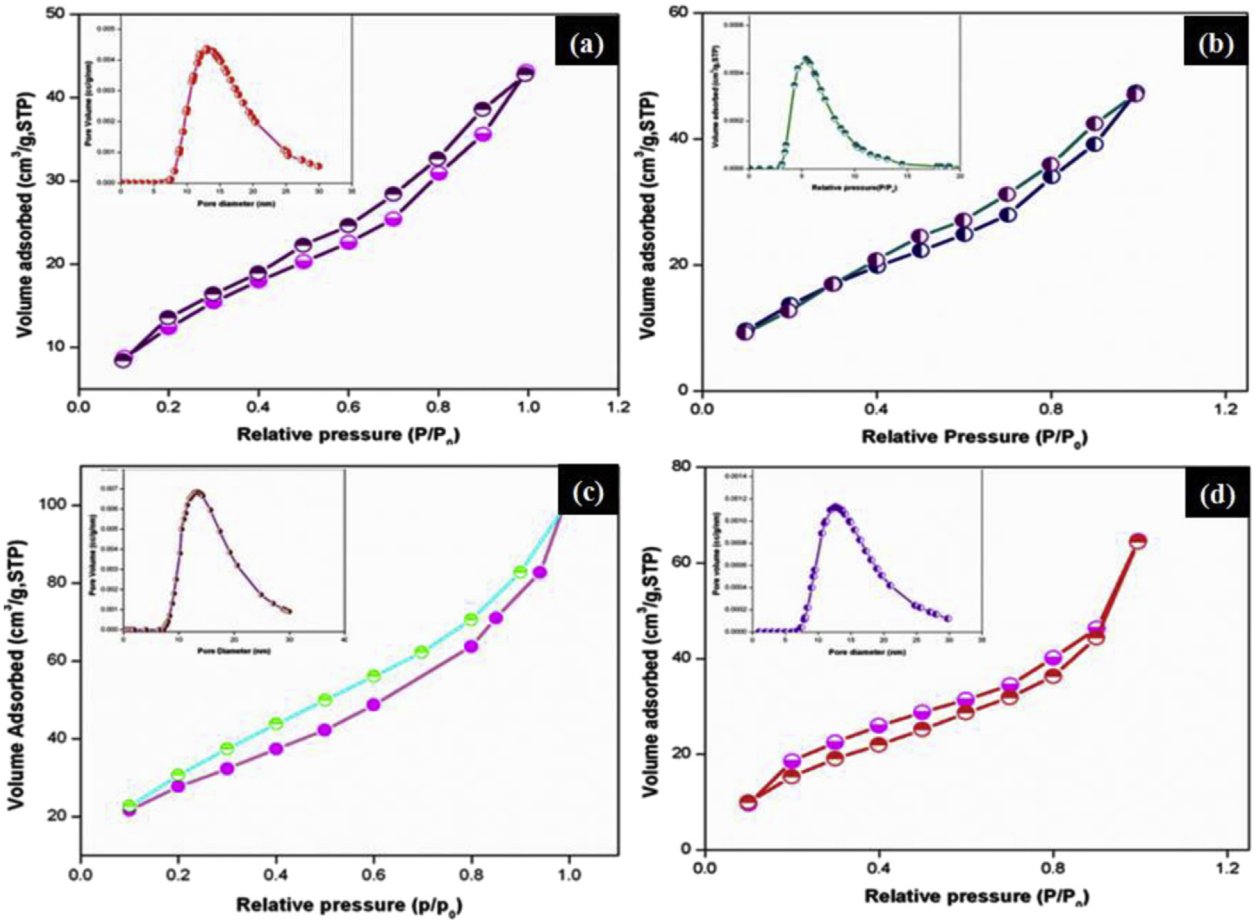

Fig. 4. Nitrogen adsorption-desorption isotherm of CuO nanostructures (a) Nanoflowers (b) Nanorods (c) Nanoleaves (d) Nanoflakes and (inset) the corresponding pore size distribution.

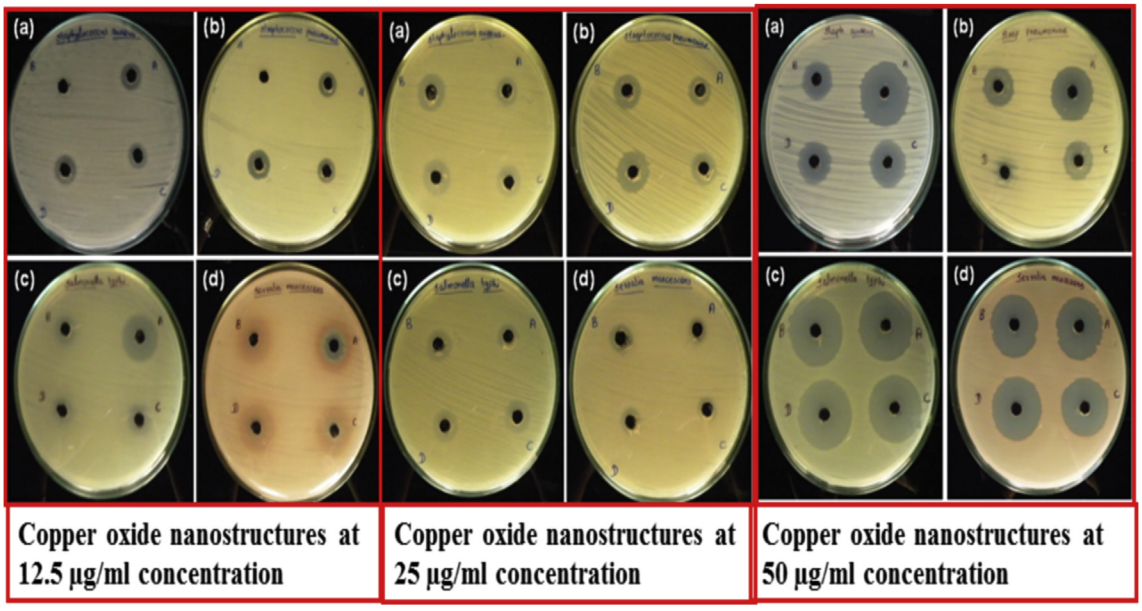

Fig. 5. Antibacterial activity of CuO nanostructures against bacterial strains a) *Staphylococcus* aureus, b) *Streptococus Pneumoniae*, c)*Salmonella typhimurium* and d) *Serratia marcescens* (Note:A-Nanoflowers, B- Nanorods, C-Nanoleaves and D-Nanoflakes).

assay. Fig. 7 shows the hemolytic activity of control and CuO nanostructures. 100% hemolysis was observed, when water is

Table 1
Zone of inhibition (in mm) of CuO nanostructures against bacterial strains.

Samples	Zone of inhibition (mm)											
	Staphylococcus aureus			*Streptococcus pneumoniae*			*Salmonella typhimurium*			*Serratia marcescens*		
	12.5 μg/ml	25 μg/ml	50 μg/ml	12.5 μg/ml	25 μg/ml	50 μg/ml	12.5 μg/ml	25 μg/ml	50 μg/ml	12.5 μg/ml	25 μg/ml	50 μg/ml
A – Nanoflowers	14	15	49	13	15	47	22	18	50	22	14	44
B – Nanorods	0	21	33	0	22	40	19	22	47	4	19	43
C – Nanoleaves	12	18	44	12	18	42	16	21	48	8	17	41
D – Nanoflakes	10	20	23	15	22	16	14	19	47	12	15	42

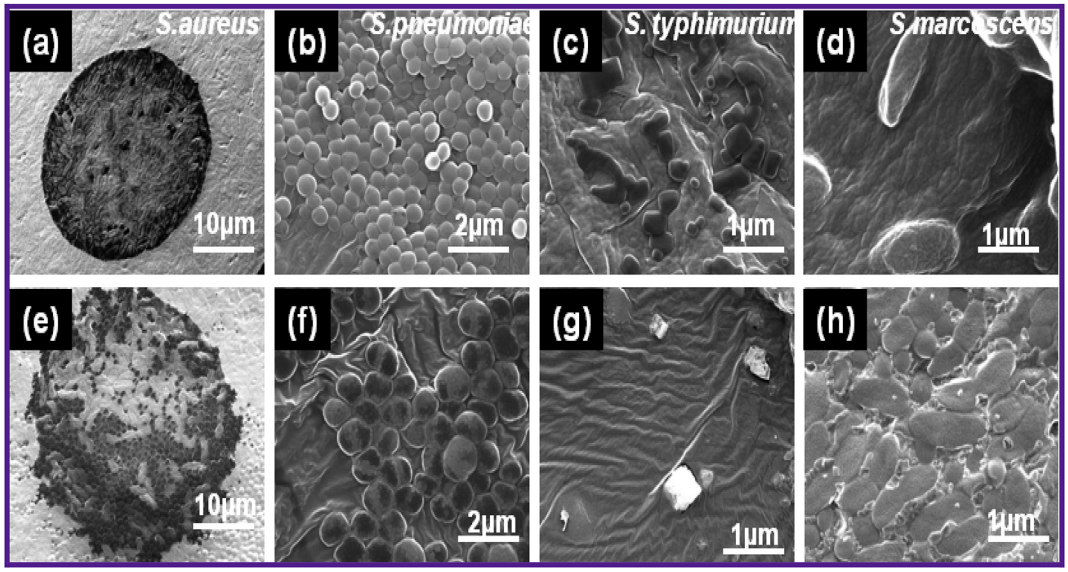

Fig. 6. Morphological behavior of bacteria (a–d) before and (e–h) after exposure to nanostructures.

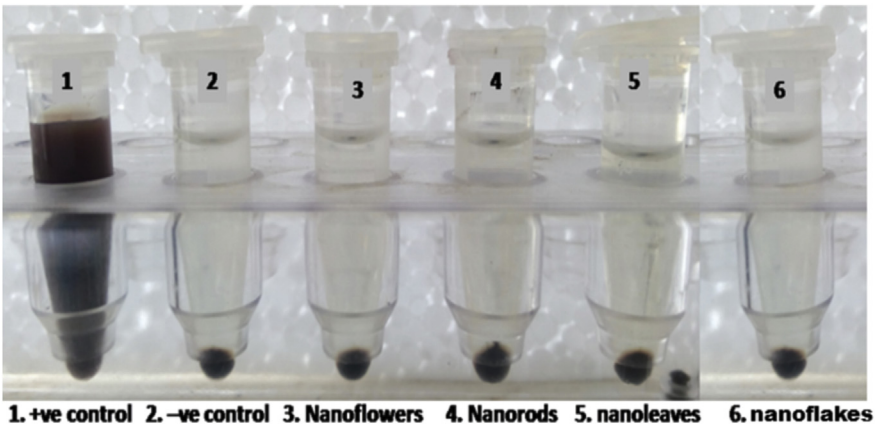

Fig. 7. Haemolytic activity of CuO nanostructures.

Table 2
Haemolytic activity of CuO nanostructures towards goat blood.

Samples	Absorbance values	Haemolysis (%)
RBC (+ve control)	1.548	100
PBS (–ve control)	0.026	0.8
Nanoflowers	0.051	1.64
Nanorods	0.046	1.31
Nanoleaves	0.038	0.78
Nanoflakes	0.049	1.5

added to RBC (+ve control). RBC in PBS solution showed only 0.8% hemolysis and it is taken as negative control. The absorbance values of nanostructures in RBC were less than 5% (Table 2.) and it is comparable to the ⁻ve control. Hence, the prepared nanostructures are hemocompatible or biocompatible and can be used as an antibacterial agents.

5. Conclusion

In the present study, three different CuO nanostructures namely,

nanoleaves, nanoflowers and nanoflakes have been synthesized by well controlled hydrothermal reaction and the fourth nanostructure, the nanorods has been synthesized by room temperature sonochemical method. By varying the preparatory conditions, such as, reactants and additives, a precise control on the morphology of the samples were explored. X-ray diffraction and FTIR studies confirmed that the synthesized morphologies are cupric oxide (CuO). Morphologies of the prepared CuO have been analyzed through FESEM analysis and stability by zeta potential analysis. The findings of the present work proved that the prepared CuO nanostructures are highly stable in aqueous solution and biocompatible in blood. They also exhibited pronounced bactericidal activity towards both Gram positive and Gram negative bacteria. Our results suggested that the synthesized CuO nanostructures have a potential application as an antibacterial agent and may have future applications in the development of antibiotics to control infections caused by a variety of bacterial strains.

References

[1] C. Shiguo, C. Shaojun, J. Song, X. Meiling, L. Junxuan, T. Jiaoning, G. Zaochuan, ACS Appl. Mater. Interfaces 3 (2011) 1154–1162.
[2] J.B. Reitz, E.I. Solomon, J. Am. Chem. Soc. 120 (1998) 11467–11471.
[3] B. Pandi, G.P. Halliah, M. Jayaraman, Colloids Surf. B Biointerfaces 103 (2013) 9–14.
[4] K.D. Raj, P. Bhavani, Nenavathu, T. Soumita, Colloids Surf. B Biointerfaces 114 (2014) 218–224.
[5] B. Niranjan, M. Satyabadi, S. Umakanta, P. Kulamani, Ind. Eng. Chem. Res. 50 (2011) 9479–9486.
[6] E. Nuengruethai, T. Titipun, T. Somchai, Appl. Surf. Sci. 277 (2013) 211–217.
[7] M.V. Canamares, J.V.G. Ramos, J.D.G. Varga, C. Domingo, Langmuir 21 (2005) 8546–8553.
[8] S. Sonia, S. Poongodi, P.S. Kumar, D. Mangalaraj, N. Ponpandian, C. Viswanathan, Mat. Sci. Semi. Process. 30 (2015) 585–591.
[9] S. Sonia, S. Jayram, S. Kumar, S. Mangalaraj, S. Ponpandian, S. Viswanathan, Superlat. Microstruct. 66 (2014) 1–9.
[10] S. Sonia, P.S. Kumar, D. Mangalaraj, N. Ponpandian, C. Viswanathan, Appl. Surf Sci. 283 (2013) 802–807.
[11] A. Mclaren, T.V. Solis, G. Li, S.C. Tsang, J. Am. Chem. Soc. 131 (2009) 12540–12541.
[12] Y. Fan, R. Liu, W. Du, Q. Lu, H. Pang, F. Gao, J. Mater. Chem. 22 (2012) 12609–12613.
[13] K. Karthikeyan, V. Murugan, Z. Ling-He, Y. Kyusik, J.K. Sang, J. Phys. Chem. C 116 (2012) 17280–17287.
[14] S. Wang, H. Xu, H. Qian, J. Wang, Y. Liu, W. Tang, J. Solid State Chem. 182 (2009) 1088–1093.
[15] J.B. Liang, J.B. Liu, Q. Xie, S. Bai, W.C. Yu, Y.T. Qian, J. Phys. Chem. B 109 (2005) 9463–9467.
[16] J.S. Tawale, K. Dey, R. Pasricha, K.N. Srivastava, Thin Solid Films 519 (2010) 1237–1244.
[17] Y. Zhao, J. Zhao, Y. Li, D. Ma, S. Hou, L. Li, X. Hao, Z. Wang, Nanotechnology 22 (2011) 115604–115609.
[18] H. Xiao, S. Fu, L. Zhu, Y. Li, G. Yang, J. Eur. Inorg. Chem. 56 (2007) 1966–1971.
[19] Y. Peng, A.W. Xu, B. Deng, M. Antonietti, H. Colfen, J. Phys. Chem. B 110 (2006) 2988–2993.
[20] Y. Li, X.Y. Yang, J. Rooke, G.V. Tendeloo, Su BL, J. Colloid Interfaces Sci. 348 (2010) 303–312.
[21] J. Lovric, S.J. Cho, F.M. Winnik, D. Maysinger, Chem. Biol. 12 (2005) 1227–1234.
[22] M. Keisuke, S. Kazuko, M. Ken, M. Fumitaka, J. Phys. Chem. A 117 (2013) 10145–10150.